Accepted Manuscript

Journal of the Geological Society

Remobilization of inverted normal faults drives active extension in the axial zone of the southern Apennine mountain belt (Italy)

G. Camanni, G. De Landro, S. Mazzoli, M. Michele, T. Muzellec, A. Ascione, D. P. Schaff, S. Tarantino & A. Zollo

DOI: https://doi.org/10.1144/jgs2024-184

To access the most recent version of this article, please click the DOI URL in the line above. When citing this article please include the above DOI.

Received 6 September 2024
Revised 14 November 2024
Accepted 19 November 2024

Supplementary material at https://doi.org/10.6084/m9.figshare.c.7401635

Remobilization of inverted normal faults drives active extension in the axial zone of the southern Apennine mountain belt (Italy)

G. Camanni[1], G. De Landro[2,*], S. Mazzoli[3], M. Michele[4], T. Muzellec[2], A. Ascione[1], D. P. Schaff [5], S. Tarantino[6], A. Zollo[2]

[1] DiSTAR, Università degli Studi di Napoli "Federico II", Naples, Italy

[2] RISSC-Lab, Dipartimento di Fisica E. Pancini, Università degli Studi di Napoli "Federico II", Naples, Italy

[3] School of Science and Technology - Geology Division, University of Camerino, Camerino, Italy

[4] Istituto Nazionale di Geofisica e Vulcanologia, Rome, Italy

[5] Lamont-Doherty Earth Observatory of Columbia University, Palisades, NY, USA

[6] Istituto Nazionale di Geofisica e Vulcanologia, L'Aquila, Italy

Corresponding author: Grazia De Landro (grazia.delandro@unina.it)

Abstract

The Irpinia region is one of the most seismically active areas of Italy due to ongoing, late-orogenic extension in the axial zone of the Apennine mountain belt. However, the 3D architecture and the nature of the faults that drive this extension are still uncertain, posing challenges to seismic hazard assessment. Here, we address these uncertainties by integrating a new catalogue of high-resolution micro-seismicity (M_L<3.5) complemented by earthquake focal mechanisms, with existing 3D seismic velocity models and geological data. We found that micro-seismicity is primarily taking place along a segmented, approximately 60 km long, deep-seated, Mesozoic normal fault that was inverted during the shortening stages of the Apennine orogeny and then extensionally reactivated during the Quaternary. These findings suggest that multiple events of reactivation of long-lived faults can weaken their strength, making them prone to co-seismic remobilization under newly imposed strain fields in active mountain belts.

1. Introduction

The Irpinia region, located in the axial zone of the Neogene southern Apennines mountain belt (e.g., Ippolito et al., 1975; Roure et al., 1991; Cello and Mazzoli, 1999; Pescatore et al., 1999; Menardi Noguera and Rea, 2000; Patacca and Scandone, 2007; Ciarcia and Vitale, 2024), is one of the most seismically active areas of Italy, due to ongoing, late-orogenic extension (~3 mm/yr, D'Agostino, 2014; e.g., Ascione et al., 2013 and references therein). In 1980, the Irpinia region was struck by a M_S 6.9 earthquake (the largest Italian event in the last 100 years) that originated from a complex multi-segment rupture process (e.g., Bernard and Zollo, 1989) and caused severe damage and thousands of fatalities in a wide epicentral area. During the last four decades, a moderate aftershock and background seismicity has continuously affected the crustal volume delimited by the faults that were activated during the 1980 M_S 6.9 Irpinia earthquake (e.g., De Matteis et al., 2012; Amoroso et al., 2014). Furthermore, since 2005, the monitoring of the Irpinia region by dense seismic networks (Irpinia Seismic Network, ISNet, and the Istituto Nazionale di Geofisica e Vulcanologia network, INGV) revealed the occurrence of persistent seismicity with magnitude near 0 (De Landro et al., 2015; Amoroso et al. 2017;

D'Agostino et al. 2018; Festa et al. 2021; Picozzi et al. 2019; Palo et al. 2023a, 2023b; Scotto di Uccio, 2024).

However, the 3D architecture and the nature of the faults that are being remobilized nowadays, which may control this seismicity and drive the ongoing extension, are not yet well-understood. These uncertainties pose significant challenges for seismic hazard assessment in this highly active and densely populated region of southern Italy. In this work, we address these uncertainties by the integrated analysis of a newly reconstructed, high-resolution catalogue of approximately 15 years of micro-seismicity (M_L<3.5) complemented by newly calculated and compiled earthquake focal mechanisms, with existing 3D seismic velocity models (De Landro et al., 2022), and available geological models based on surface geology and seismic interpretation (e.g., Ascione et al., 2013, 2020).

2. Geological structure and evolution of the axial zone of the southern Apennines

The architecture of the axial zone of the southern Apennines is characterized by a two-layer structure (Mazzoli et al., 2014; **Fig. 1**). The upper layer consists of a far-travelled (> 50 km) allochthonous assemblage forming an intensely deformed, thin-skinned fold and thrust belt. This overlies a less deformed, thick-skinned lower layer. The thin-skinned belt primarily involves Mesozoic-Cenozoic successions of the Apennine Platform (shallow-water carbonates) and of the Lagonegro Basin (shallow-water to pelagic limestones, radiolarian cherts and shales). Conversely, the deeper thick-skinned belt involves the 6 to 8 km thick shallow-water carbonate succession of the Apulian Platform, as well as the Lower Triassic siliciclastic deposits located at its base and the underlying basement. The recent tectonic emplacement of the thin-skinned belt is testified by the occurrence, in its footwall, of Pliocene to Lower Pleistocene foreland basin deposits resting on top of the Apulian Platform carbonates and penetrated by numerous oil wells (Mazzoli et al., 2001). Since the middle Pleistocene the axial zone of the southern Apennines is undergoing a phase of late-orogenic extension (Cello et al., 1982; Cinque et al., 1993; Hippolyte et al., 1994; Butler et al., 2004; Caiazzo et al., 2006). This extension led to the development of neo-formed, Quaternary extensional faults that dissect the mountain belt (black faults in the section of **Fig. 1**) and is responsible for the ongoing seismicity within the study area.

Importantly for this work, the thick-skinned belt (where the seismicity is mostly focused) is comprised of deep-seated, steeply-dipping reverse faults mainly formed by the reverse/oblique-slip reactivation ('inversion') of pre-existing Mesozoic normal faults (Butler et al., 2004; Shiner et al., 2004; Mazzoli et al., 2000, 2008; Ascione et al., 2013, 2020; Amoroso et al., 2014, 2017). These structures control the so-called Apulian inversion belt (Mazzoli et al., 2008). The inversion tectonics model for the Apulian Platform shortening-related structures was derived by the interpretation of high-resolution seismic reflection profiles calibrated with numerous oil wells and subsequent depth conversion, cross-section balancing and restoration (e.g., Shiner et al., 2004). Shortening-related reactivation of inherited faults in the Apulian Platform carbonates was unravelled by the interpretation of high-quality seismic data also in the outer zone of the southern Apennines by Bitonte et al. (2021). The latter authors also documented fault propagation into the foreland basin deposits as a result of such fault reactivation. Within the study area, the development of the Apulian inversion belt was controlled by the reverse/oblique-slip reactivation of a SW-dipping Mesozoic normal fault (red fault in the cross-section of **Fig. 1**). This structure produced a prominent uplift of the Apulian Platform carbonates in its hanging wall (Ascione et al., 2013, 2020). The carbonate culmination is dissected by a deeply rooted Quaternary horst, which NW-dipping boundary fault was associated with the Ms 6.9 main shock of the 1980 Irpinia earthquake (Ascione et al., 2013, 2020; Amoroso et al., 2014).

3. Seismological data and methods

The micro-seismicity catalogue at the base of this work was obtained by analysing a data set consisting of about 2400 micro-earthquakes, with local magnitude (M_L) ranging between 0.5 and 3.2. These events were recorded by 42 ISNet and INGV stations from August 2005 to December 2022. We used manually picked first *P*- and *S*-wave arrival times from ISNet bulletin (http://isnet-bulletin.fisica.unina.it/cgi-bin/isnet-events/isnet.cgi) and integrated manually picks from INGV stations (see **SM1** in Supplementary Material). Initially, we located the events with a probabilistic method (NLLoc, Lomax et al. 2009) and a 3D velocity model optimized for the area (De Landro et al., 2022), which allowed to obtain a first location catalogue with an average RMS residual of 0.15 s and horizontal location errors within 1.5 km (average 800 m) and vertical location errors within 2 km (average 1.2 km) for the 85% of events. Successively, we refined the absolute 3D location with the double-difference approach

(HypoDD, Waldauser & Ellswort, 2000) by using catalogue (CT) and cross-correlation (CC) differential times (Schaff & Waldauser, 2005). The final residual RMS was 0.008 s for CC data and 0.03 s for CT data. The final horizontal and vertical location errors were within 100 meters for most of the events. For further details on the used location strategy and method see **SM2** in Supplementary Material. The final dataset is available in De Landro (2024).

As a further constraint on the fault geometry and kinematics, the composite focal mechanisms of significant clusters of this new micro-seismicity catalogue were also calculated using the consolidated code FPFIT (Reasenberg, 1985). Similarly to Festa et al. (2021) and Muzellec et al. (2023), we evaluated, for four selected hypocentre clusters, the composite focal mechanisms (red "beach ball" in **Fig. 2**) by integrating the polarities of co-located events for the construction of more constrained mechanisms. Furthermore, where it was not possible to calculate composite focal mechanisms due to the lack of hypocentre clusters, we integrated four additional focal mechanisms of single events (dark grey "beach ball" in **Fig. 2**). These were selected among the focal mechanisms available from the ISNet bulletin and refined by using the 3D location. To validate this selection, we compared them with those obtained by De Matteis et al. (2012), in which the author performed an extensive analysis of focal mechanisms and refined the stress field of the Irpinia region. For further details on focal mechanism data, calculation, evaluation and selection, and uncertainties see **SM3** and **Table SM3** in Supplementary Material and De Landro (2024).

As a constraint on the depth and geometry of the top of the Apulian Platform carbonates, we used the 3D P-wave velocity model of De Landro et al. (2022). This model was built using a linearized, tomographic approach in which about 13000 P- and S-wave arrival times were inverted to retrieve, jointly, the location of about 1500 earthquakes of ISNet catalogue and the P- and S-phases velocity parameters. Similarly to Amoroso et al. (2014, 2017), a multi-scale strategy was applied starting from a coarser parameterization up to a finer one of 3x3x1 km^3, with a forward grid of 500 m of step. The model resolution was assessed with the integration of the resolution matrix, composed by intrinsic resolution and spreading function, and the density of ray around each node.

4. Spatial distribution of micro-seismicity and P-wave velocities

Earthquake hypocentres within the study area mostly extend from about 3 km to 14 km depth and are generally distributed along an about 20 km wide, 60 km long, NW-SE-elongated belt (**Figs. 1, 2**). Within this distribution, distinct features can be recognized from horizontal and vertical sections through the data.

On horizontal sections (**Fig. 2A**), from approximately 10 km depth and downward, hypocentres are roughly aligned along two NW-SE-elongated clusters, each ca. 5 km to 10 wide and ca. 30 km long (see red dashed lines in **Fig. 2A**). These two clusters are arranged in a geometry in which a SE cluster steps NW-ward to the right into a NW cluster, the latter being associated with the largest concentration of hypocentres. Notably, at all depths, the volume in which this step occurs is characterized by a decreased density of hypocentres. From approximately 8 km depth and upwards, these two clusters become shorter and less clearly defined while another NW-SE-elongated cluster more prominently emerges located to the SW of the NW cluster. This other cluster is ca. 5 to 10 km wide and 30 km long, being best identifiable on the 8 km and 6 km depth horizontal sections (see blue dashed lines in **Fig. 2A**).

On vertical sections perpendicular to the NW-SE map-view clusters (i.e., NE-SW; **Fig. 2B**), earthquake hypocentres forming the two major, right-stepping map-view clusters overall align into a primary, locally discontinuous, SW-dipping cluster ca. 5 to 10 km wide, recognizable throughout the study area (see red dashed lines in **Fig. 2B**). This cluster widens upwards near the centre of the study area (section III in **Fig. 2B**). In contrast, the shallower NW-SE-elongated cluster in the NE sector of the study area corresponds to a NW-dipping, ca. 5 to 10 km wide cluster in cross-section (see blue dashed lines in **Fig. 2B**).

From approximately 10 km depth upwards on horizontal sections, the two major NW-SE-elongated hypocentre clusters roughly coincide with a distinct NW-SE boundary in the P-wave velocity model, between higher velocities in the SW and lower velocities in the NE (**Fig. 2A**). In all vertical sections, this feature manifests as a prominent deepening of low P-wave

velocities from SW to NW (**Fig. 2B**). This is best highlighted by the 4.5 km/s, 5 km/s and 5.5 km/s isovelocity contours and approximately occurs across the primary SW-dipping cluster of hypocentres (**Fig. 2B**). It is worth noting that this deepening is largest in the central and north-western parts of the study area (**Fig. 2**).

In the 10 km, 8 km, and 6 km depth sections (**Fig. 2A**), the boundary between higher and lower velocities shows a curved morphology in map view, taking on a more N-S orientation at the location of the step between the two deep NW-SE-elongated hypocentre clusters. This curved deepening of low velocities is clearly depicted by the 5.5 km/s isovelocity surface (**Fig. 3**).

5. Earthquake focal mechanisms

The four composite and the four compiled, single event earthquake focal mechanisms within the study area all display an approximately pure dip-slip, extensional kinematics (**Fig. 2 A, B;** see also De Landro, 2024 and **Table SM3** in Supplementary Material), in agreement with the regional strain field of the study area (De Matteis et al., 2012; Festa et al., 2021; Bello et al., 2021; Ricigliano Eqk report, RISSC-Lab 2024). In general, each focal mechanism has nodal planes striking roughly NW-SE sub-parallel to the overall orientation of the earthquake hypocentre clusters, although minor variations to these orientations exist. For example, some focal mechanisms include an about N-S-oriented nodal plane (e.g., focal mechanisms 1, 3, 5, 7, 8, **Fig. 2A**), while others include an approximately E-W-oriented nodal plane (e.g., focal mechanism 2, **Fig. 2A**). Dip angles of the focal mechanism nodal planes are also overall consistent with the dip of the main earthquake hypocentre clusters (i.e., either SW- or NE-dipping; **Fig. 2B**). However, while some focal mechanisms are associated with two moderately dipping nodal planes (e.g., focal mechanisms 2, 3, 7, 8, **Fig. 2B**), others display a pair of nodal planes in which one is steeply dipping and the other one is gently dipping (focal mechanisms 1, 4, 5, 6, **Fig. 2B**).

6. Discussion and conclusions

As we have seen, the deep geological structure within the study area is that of an Apulian Platform carbonates culmination bounded in the NE by, and uplifted along, an inverted Mesozoic normal fault (cross-section in **Fig. 1**). When integrating the seismological data presented above with this geological information, several coherent features become apparent (**Fig. 4**). In particular, (i) the shallow high P-wave velocities nearly coincide with the uplifted Apulian Platform carbonates, and (ii) the primary SW-dipping cluster of hypocentres approximately aligns with the inverted Mesozoic normal fault (red fault in the section of **Fig. 1**) responsible for this uplift. Since both seismological features are recognizable throughout the study area, we infer that a structural model in which Apulian Platform carbonates are uplifted along an inverted SW-dipping Mesozoic normal fault holds for the entire study area (**Fig. 4**). Furthermore, considering that both earthquake hypocentres and P-wave velocities are right-stepped (**Figs. 2** and **3**), the inverted fault may be confidently interpreted as also stepped in map view (**Fig. 4**). This is further supported by results of gravity data modelling (Improta et al., 2003; see also De Landro et al., 2015), which show that the depocenter ahead of the inverted fault is also right-stepped in map view. This feature most likely reflects the original segmentation of the precursor normal fault, which comprised two fault segments separated by a relay zone (e.g., Camanni et al., 2023, and references therein).

The inverted Mesozoic normal fault coincides both in map view and cross-section with an approximately 5 to 10 km wide zone of earthquake hypocentres (**Figs. 2** and **4**), rather than with a well-delineated feature. We interpret this as due to the combined effect of this structure being likely a broad fault zone (a common feature for faults, e.g., Childs et al., 2009) rather than an individual fault surface (see also De Matteis et al., 2012 for a similar interpretation of the micro-seismicity in the Irpinia region), and of the uncertainty in the event's location. However, the overall dip and strike of the fault zone is well-consistent with that of the nodal planes of the focal mechanisms (i.e., NW-SE striking and SW-dipping, **Fig. 4**).

For the northern part of the study area (i.e., north of the step of the inverted fault), the attitude of the faults included in this new structural model (**Fig. 4**) is consistent with that derived from the 0 s and 40 s sub-events of the 1980 Irpinia earthquake (Westaway and Jackson, 1984; Bernard and Zollo, 1989; Pantosti and Valensise, 1990; Pingue et al., 1993; Amoruso et al., 2005, 2011). On the other hand, for the southern part of the study area this new structural model is consistent with the minority interpretation provided by Amoruso et al. (2005, 2011) for the

20 s sub-event (which most authors interpreted to have occurred along a NE-dipping fault, in some case interpreted to be low angle, e.g., Bernard and Zollo, 1989).

The micro-seismicity within the study area is associated with ongoing late-orogenic extension, in agreement with focal mechanisms that display normal sense kinematics (e.g., this study; De Matteis et al. 2012; Festa et al. 2021; **Fig. 4**). This may appear counterintuitive, since we found that most seismicity is taking place along an inverted fault that preserves its reverse net displacement associated with the uplift of Apulian Platform carbonates (**Figs. 1** and **4**). This fault is long-lived and has been active with a normal sense of movement in the Mesozoic and reactivated with a reverse/oblique-slip kinematics during the Apennine orogeny. We suggest that these multiple slip events weakened the strength of the fault, making it prone to further remobilization ('negative inversion') under the newly-imposed extensional strain field affecting the Irpinia region. While in the SE part of the study area this is the only fault driving ongoing extension, in the NW sector this fault is acting in association with two further neo-formed faults that define a Quaternary horst within the Apulian Platform carbonates (one of these two faults, i.e. the NE dipping one, generated the Ms 6.9 main shock of the 1980 Irpinia earthquake and contains most of the micro-seismicity; **Fig. 4**). This occurs in a sector where the net displacement of the inverted fault is maximum, as shown by the highest deepening of P-wave velocities that define the deepest top Apulian Platform carbonates in the fault footwall; **Fig. 2**). Based on this observation, we suggest that the need for extensional readjustment is most pronounced in this sector, thus requiring the involvement of all three faults.

These findings have broader implications for other active mountain belts characterized by a thick-skinned style of deformation and inversion tectonics (e.g., Taiwan: Lacombe and Mouthereau, 2002, Camanni et al., 2014, 2016; Western Alps: Mosar et al., 1999; Zagros: Tavani et al., 2020). When assessing seismic hazard in such mountain belts, particular attention should be directed towards long-lived faults. The results of this work also indicate that this should be done regardless of the consistency between the geological displacement of the fault and the kinematics of the newly-imposed strain field.

Acknowledgments

We thank the Irpinia Near Fault Observatory revision team that works on the INFO bulletin construction (http://isnet-bulletin.fisica.unina.it/cgi-bin/isnet-events/isnet.cgi). The authors acknowledge financial support from the Project TRHAM - “Relation Between 3d Thermo-Rheological Model And Seismic Hazard For The Risk Mitigation In The Urban Areas Of Southern Italy" funded by the European Union - Next Generation EU, Mission 4, Component 2 - CUP B53D23033710001 - Grant Number P2022P37SN. The authors acknowledge financial support from the Project FRACTURES - “Multiscale study of seismogenic processes in Campania-Lucania Apennines using machine learning algorithms and multiparametric observations" funded by the European Union - Next Generation EU, Mission 4, Component 2 - CUP B53D23006980006 - Grant Number 2022BEKFN2. The work of AZ was supported in part by Project “PE0000005–RETURN-SPOKE 3-CUP UNINA: E63C220002000002”. The code FPFIT (Reasenberg, 1985) was used for calculating the composite focal mechanisms. The Generic Mapping Tools (GMT) version 4 (Wessel et al., 2019), licensed under LGPL version 3 or later and available at https://www.generic-mapping-tools.org/, were used to produce some of the figures. Two anonymous reviewers and the Journal of the Geological Society Editors are also acknowledged.

Data Availability Statement

The micro-seismicity catalogue and the focal mechanisms used in this study are stored in the following repository under the CC BY 4.0 license: https://zenodo.org/records/11208080 (De Landro., 2024). The 3D P-wave velocity model used in this study is available through De Landro et al. (2022). This study used the Irpinia Near Fault Observatory (https://isnet.unina.it) data and products. Seismic data were available at the EIDA website (https://eida.ingv.it/it/) and at the EPOS Data Portal (https://www.epos-eu.org/dataportal) – IRPINIA Seismic Velocity and Acceleration Waveforms (Continuous) provided by Università di Napoli Federico II and INGV, networks IX and IV. Bullettin Seismic catalogue was available at the Irpinia Near Fault Observatory website (http://isnet-bulletin.fisica.unina.it/cgi-bin/isnet-events/isnet.cgi) and at the EPOS Data Portal (https://www.epos-eu.org/dataportal) – IRPINIA Seismic Events provided by Università di Napoli Federico II.

Competing Interests Statement

The authors declare that they have no known competing financial interests or personal relationships that could have appeared to influence the work reported in this paper.

References

Amoroso O., Ascione A., Mazzoli S., Virieux J. & Zollo A. (2014), Seismic imaging of a fluid storage in the actively extending Apennine mountain belt, southern Italy. *Geophysical Research Letters, 41,* 3802–3809. doi: 10.1002/2014GL060070

Amoroso O., Russo G., De Landro G., Zollo A., Garambois S., Mazzoli, S., Parente, M. & Virieux J. (2017), From Velocity and Attenuation Tomographies to Rock Physical Modeling: Inferences on fluid-driven earthquake processes at the Irpinia fault system in Southern Italy. *Geophysical Research Letters, 44 (13),* 6752-6760. doi: 10.1002/2016GL072346

Amoruso, A., Crescentini, L., and Scarpa, R. (2005), Faulting geometry for the complex 1980 campania-lucania earthquake from levelling data. *Geophys. J. Int., 162,* 156–168. doi:10.1111/j.1365-246X.2005.02652.x

Amoruso, A., Crescentini, L., Di Lieto, B., and Scarpa, R. (2011), Faulting mechanism of the campania–lucania 1980 earthquake, Italy, from high-resolution, 3D velocity structure, aftershock relocation, fault-plane solutions, and post-seismic deformation modeling. *Ann. Geophys 54,* 806–821. doi:10.4401/ag-4984

Ascione A., Mazzoli S., Petrosino P. and Valente E. (2013), A decoupled kinematic model for active normal faults: Insights from the 1980, MS = 6.9 Irpinia earthquake, southern Italy. *Geological Society of America Bulletin, 125,* 1239-1259. doi: 10.1130/B30814.1

Ascione, A., Nardò, S. and Mazzoli, S. (2020), The MS 6.9, 1980 Irpinia Earthquake from the Basement to the Surface: A Review of Tectonic Geomorphology and Geophysical Constraints, and New Data on Post-seismic Deformation. *Geosciences, 10, 493*. doi: 10.3390/geosciences10120493

Bello, S., de Nardis, R., Scarpa, R., Brozzetti, F., Cirillo, D., Ferrarini, F., Di Lieto, B., Arrowsmith, R. J., and Lavecchia, G. (2021), Fault pattern and seismotectonic style of the Campania–Lucania 1980 earthquake (Mw 6.9, Southern Italy): New multidisciplinary constraints. *Frontiers in Earth Science, 8*. doi: 10.3389/feart.2020.608063

Bernard, P., and Zollo, A. (1989), The Irpinia (Italy) 1980 earthquake: detailed analysis of a complex normal faulting. *J. Geophys. Res 94,* 1631–1647. doi:10.1029/jb094ib02p01631

Bitonte, R., Livio, F. A., Mazzoli, S., Bellentani, G., Di Cesare, L., Dall'Igna, M., Castelluccio, A., and Scaramuzzo, E. (2021), Frontal accretion vs. foreland plate deformation: Discriminating the style of

post-collisional shortening in the Apennines. *Journal of Structural Geology 145*, 104290. doi: 10.1016/j.jsg.2021.104290

Butler, R.W.H., Mazzoli, S., Corrado, S., De Donatis, M., Di Bucci, D., Gambini, R., Naso, G., Nicolai, C., Scrocca, D., Shiner, P., and Zucconi, V. (2004), Applying thick-skinned tectonic models to the Apennine thrust belt of Italy: Limitations and implications, in McClay, K.R., ed., Thrust Tectonics and Petroleum Systems: *American Association of Petroleum Geologists Memoir 82*, 647–667. doi: 10.1306/M82813C34

Camanni, G., C.-H. Chen, D. Brown, J. Alvarez-Marron, Y.-M. Wu, H.-A. Chen, H.-H. Huang, H.-T. Chu, M.-M. Chen, and C.-H. Chang (2014), Basin inversion in central Taiwan and its importance for seismic hazard. *Geology, 42*, 147-150. doi: 10.1130/G35102.1

Camanni, G., J. Alvarez-Marron, D. Brown, C. Ayala, Y.-M. Wu, and H.-H. Hsieh (2016), The deep structure of south-central Taiwan illuminated by seismic tomography and earthquake hypocentre data. *Tectonophysics, 679*, 235-245. doi: 10.1016/j.tecto.2015.09.016

Camanni, G., Freda, G., Delogkos, E, Nicol, A., and Childs, C. (2023), 3D geometry and displacement transfer of an oblique relay zone on outcropping normal faults. *Journal of Structural Geology*, 177. doi: 10.1016/j.jsg.2023.105001

Caiazzo, C., Ascione, A., and Cinque, A. (2006), Late Tertiary–Quaternary tectonics of the southern Apennines (Italy): New evidences from the Tyrrhenian slope. *Tectonophysics, 421*, 23–51, doi:10.1016/j.tecto.2006.04.011

Cello, G., Guerra, I., Tortorici, L., Turco, E., and Scarpa, R. (1982), Geometry of the neotectonic stress field in southern Italy: Geological and seismological evidence. J*ournal of Structural Geology, 4*, 385–393. doi: 10.1016/0191-8141(82)90030-X

Cello, G., Mazzoli, S. (1999), Apennine tectonics in southern Italy: a review. *Journal of Geodynamics 27*, 191–211. doi: 10.1016/S0264-3707(97)00072-0

Chatelain, J. L. (1978), Etude fine de la sismicité en zone de collision continentale à l'aide d'un réseau de statios portables: La region Hindu-Kush-Pamir, thèse de 3 éme cycle. Univ. Paul Sabatier, Toulouse, France

Childs, C., Manzocchi, T., Walsh, J.J., Bonson, C.G., Nicol, A., Schöpfer, M.P.J. (2009), A geometric model of fault zone and fault rock thickness variations. *Journal of Structural Geology, 31*, 117–127. doi: 10.1016/j.jsg.2008.08.009

Ciarcia, S., and Vitale, S. (2024), Orogenic evolution of the northern Calabria–southern Apennines system in the framework of the Alpine chains in the central-western Mediterranean area. *Geological Society of America Bulletin.* doi: 10.1130/B37474.1

Cinque, A., Patacca, E., Scandone, P., and Tozzi, M. (1993), Quaternary kinematic evolution of the southern Apennines. Relationships between surface geological features and deep lithospheric structures. *Annals of Geophysics, 36*, 249–260. doi: 10.4401/ag-4283

D'Agostino, N., Silverii, F., Amoroso, O., Convertito, V., Fiorillo, F., Ventafridda, G. and Zollo, A. (2018), Crustal deformation and seismicity modulated by groundwater recharge of karst aquifers. *Geophysical Research Letters, 45(22)*, 12-253. doi: 10.1029/2018GL079794

D'Agostino, N. (2014), Complete seismic release of tectonic strain and earthquake recurrence in the Apennines (Italy). *Geophysical Research Letters, 41(4)*, 1155-1162. doi: 10.1002/2014GL059230

De Landro, G., Amoroso, O., Stabile, T., A., Matrullo, E., Lomax, A., Zollo, A. (2015), High-precision differential earthquake location in 3-D models: evidence for a rheological barrier controlling the microseismicity at the Irpinia fault zone in southern Apennines. *Geophysical Journal International, 203 (3)*, 1821–1831. doi: 10.1093/gji/ggv397

De Landro, G., Amoroso, O., Russo, G., D'Agostino, N., Esposito, R., Emolo, A., Zollo, A. (2022), Decade-long monitoring of seismic velocity changes at the Irpinia fault system (southern Italy) reveals pore pressure pulsations. *Scientific Reports, 12.* doi: 10.1038/s41598-022-05365-x

De Landro, G. (2024), Catalog of 3D DD Locations of the Irpinia Micro-Seismicity from 2008 to 2022. Zenodo. doi: https://doi.org/10.5281/zenodo.11208080

De Matteis, R., Matrullo, E., Rivera, L., Stabile, T.A., Pasquale, G. and Zollo, A. (2012), Fault delineation and regional stress direction from the analysis of background microseismicity in the southern Apennines, Italy. *Bulletin of the Seismological Society of America*, *102(4)*, 1899-1907. doi: 10.1785/0120110225

Festa, G., Adinolfi, G.M., Caruso, A., Colombelli, S., De Landro, G., Elia, L., Emolo, A., Picozzi, M., Scala, A., Carotenuto, F. and Gammaldi, S. (2021), Insights into mechanical properties of the 1980 Irpinia fault system from the analysis of a seismic sequence. *Geosciences, 11(1)*. doi: 10.3390/geosciences11010028

Hippolyte, J.-C., Angelier, J., and Roure, F., (1994), A major geodynamic change revealed by Quaternary stress patterns in the southern Apennines (Italy). *Tectonophysics, 230*, 199–210, doi:10.1016/0040-1951(94)90135-X

Ippolito, F., D'Argenio, B., Pescatore, T., Scandone, P. (1975), Structural–stratigraphic units and tectonic framework of southern Apennines. In: Squyres C, editor. Geology of Italy. *Lybian Society of Earth Science*. Libyan Arab Republic, 1975: 317–28

Improta, L., Bonagura, M., Capuano, P. & Iannaccone, G. (2003), An integrated geophysical investigation of the upper crust in the epicentral area of the 1980, Ms = 6.9, Irpinia earthquake (Southern Italy). *Tectonophysics, 361(1–2),* 139–169. doi: 10.1016/S0040-1951(02)00588-7

Lacombe, O. & Mouthereau, F. (2002), Basement-involved shortening and deep detachment tectonics in forelands of orogens: insights from recent collision belts (Taiwan, western Alps, Pyrenees). *Tectonics, 21,* 1030. doi: 10.1029/2001TC901018

Lomax, A., Michelini, A., Curtis, A., & Meyers, R. A. (2009), Earthquake location, direct, global-search methods. *Encyclopedia of complexity and systems science, 5,* 2449-2473

Mazzoli, S., Corrado, S., De Donatis, M., Scrocca, D., Butler, R.W.H., Di Bucci, D., Naso, G., Nicolai, C., and Zucconi, V. (2000), Time and space variability of "thin-skinned" and "thick-skinned" thrust tectonics in the Apennines (Italy). *Rendiconti dell'Accademia dei Lincei, Scienze Fisiche e Naturali, serie 9, v. 11*, 5–39.

Mazzoli, S., Barkham, S., Cello, G., Gambini, R., Mattioni, L., Shiner, P., and Tondi, E. (2001), Reconstruction of continental margin architecture deformed by the contraction of the Lagonegro Basin, southern Apennines, Italy. J*ournal of the Geological Society, London, 158*, 309-319. doi: 10.1144/jgs.158.2.309

Mazzoli, S., D'Errico, M., Aldega, L., Corrado, S., Invernizzi, C., Shiner, P., and Zattin, M. (2008), Tectonic burial and "young" (<10 Ma) exhumation in the southern Apennines fold and thrust belt (Italy). *Geology, 36,* 243–246. doi:10.1130/G24344A.1

Mazzoli, S., Ascione, A., Buscher, J. T., Pignalosa, A., Valente, E., and Zattin, M. (2014), Low-angle normal faulting and focused exhumation associated with late Pliocene change in tectonic style in the southern Apennines (Italy). *Tectonics, 33*. doi:10.1002/2014TC003608

Mazzotti, A., Stucchi, E., Fradelizio, G.L., Zanzi, L., and Scandone, P. (2007). Re-processing of the CROP-04 seismic data. *Bollettino della Società Geologica Italiana, 7,* 141–153.

Menardi Noguera, A., and Rea, G. (2000), Deep structure of the Campanian-Lucanian Arc (southern Apennine, Italy). *Tectonophysics, 324(4),* 239 – 265. doi: 10.1016/S0040-1951(00)00137-2

Michele, M., Chiaraluce, L., Di Stefano, R., Waldhauser, F. (2019), Fine-scale structure of the 2016–2017 Central Italy seismic sequence from data recorded at the Italian National Network. *Journal of Geophysical Research: Solid Earth 125 (4)*. doi: 10.1029/2019JB018440

Mosar, J. (1999), Present-day and future underplating in the western Swiss Alps: reconciliation of basement/wrench-faulting and thrust detachment folding of the Jura and Molasse basin in the Alpine foreland. *Earth Planetary Science Letters, 173,* 143–55. doi: 10.1016/S0012-821X(99)00238-1

Muzellec, T., De Landro, G., Camanni, G., Adinolfi, G. M., and Zollo, A. (2024), The complex 4D multi-segmented rupture of the 2014 Mw 6.2 Northern Nagano Earthquake revealed by high-precision aftershock locations. *ESS Open Archive*. doi: 10.22541/essoar.171291607.76518097/v1

Palo, M., Picozzi, M., De Landro, G., and Zollo, A. (2023a), Microseismicity clustering and mechanic properties reveal fault segmentation in southern Italy. *Tectonophysics, 856*. doi: 10.1016/j.tecto.2023.229849

Palo, M., Scotto di Uccio, F., Picozzi, M. and Festa, G. (2023b), An Enhanced Catalog of Repeating Earthquakes on the 1980 Irpinia Fault System, Southern Italy. *Geosciences, 14(1)*. doi: 10.3390/geosciences14010008

Pantosti, D., and Valensise, G. (1990), Faulting mechanism and complexity of the november 23, 1980, campania-lucania earthquake, inferred from surface observation. *J. Geophys. Res, 95*. doi:10.1029/jb095ib10p15319

Patacca, E. (2007), Stratigraphic constraints on the CROP-04 seismic line interpretation: San Fele 1, Monte Foi 1 and San Gregorio Magno 1 wells (southern Apennines, Italy). *Bollettino della Società Geologica Italiana, 7*, 185–239

Patacca, E., and Scandone, P. (2007), Geology of the Southern Apennines. *Bollettino della Società Geologica Italiana, 7*, 75–119

Pescatore, T., Renda, P., Schiattarella, M., Tramutoli, M. (1999), Stratigraphic and structural relationships between Meso-Cenozoic Lagonegro basin and coeval carbonate platforms in southern Apennines, Italy. *Tectonophysics, 315* (issues 1–4). doi: 10.1016/S0040-1951(99)00278-4

Picozzi, M., Bindi, D., Zollo, A., Festa, G. and Spallarossa, D. (2019), Detecting long-lasting transients of earthquake activity on a fault system by monitoring apparent stress, ground motion and clustering. *Sci. Rep. 9 (1)*, 1–11. doi: 10. 1038/ s41598- 019- 52756-8

Pingue, F., De Natale, G., and Briole, P. (1993), Modelling of the 1980 Irpinia earthquake source: constraints from geodetic data. *Ann. Geofisc 36,* 27–40. doi:10.4401/ag-4296

Reasenberg, P. and Oppenheimer, D.H. (1985). FPFIT, FPPLOT and FPPAGE; Fortran computer programs for calculating and displaying earthquake fault-plane solutions (No. 85-739). US Geological Survey

RISSC-Lab. (2024, febbraio 20). RISSC-Lab Report on the Mw 3.9 Ricigliano Earthquake (Italy, 2024-02-10). Zenodo. doi:10.5281/zenodo.10657217

Roure, F., P. Casero, and Vially, R. (1991), Growth processes and melange formation in the southern Apennines accretionary wedge. *Earth Planet. Sci. Lett., 102*, 395 – 412. doi: 10.1016/0012-821X(91)90031-C

Schaff, D.P. and Waldhauser, F. (2005), Waveform cross-correlation-based differential travel-time measurements at the Northern California Seismic Network. B*ulletin of the Seismological Society of America, 95(6)*, 2446-2461. doi: 10.1785/0120040221

Scotto di Uccio, F., Michele, M., Strumia, C., Supino, M., Beroza, G.C., Chiaraluce, L., D'Agostino, N. and Festa, G. (2024), Characterization and evolution of seismic sequences in the normal fault environment of the Southern Apennines. *Journal of Geophysical Research: Solid Earth*, 129 (8). doi: 10.1029/2023JB028644

Shiner, P., Beccacini, A., and Mazzoli, S. (2004), Thin-skinned versus thick-skinned structural models for Apulian carbonate reservoirs: Constraints from the Val D'Agri Fields. *Marine and Petroleum Geology, 21*, 805–827. doi:10.1016/j.marpetgeo.2003.11

Tavani, S., Camanni, G., Nappo, M., Snidero, M., Ascione, A., Valente, E., Gharabeigli, G., Morsalnejad, D., and Mazzoli S. (2020), The Mountain Front Flexure in the Lurestan region of the Zagros belt: crustal architecture and role of structural inheritances. *Journal of Structural Geology, 135*. doi: 10.1016/j.jsg.2020.104022

Waldhauser, F. and Ellsworth, W.L. (2000), A double-difference earthquake location algorithm: Method and application to the northern Hayward fault, California. B*ulletin of the seismological society of America, 90(6)*, 1353-1368. doi: 10.1785/0120000006

Wessel, P., Luis, J. F., Uieda, L., Scharroo, R., Wobbe, F., Smith, W. H. F., and Tian, D. (2019), The Generic Mapping Tools version 6. *Geochemistry, Geophysics, Geosystems, 20*, 5556–5564. doi: 10.1029/2019GC008515

Westaway, R. and Jackson, J. (1984), Surface faulting in the southern Italian Campania-Basilicata earthquake of 23 November 1980. *Nature, 312*, 436-438. doi: 10.1038/312436a0

Figure Captions

Figure 1. Geological setting of the study area in the southern Apennines mountain belt (modified after Ascione et al., 2020). Note that the Quaternary, neo-formed normal faults are only shown in the section, which is based on the integration of surface geological data with subsurface constraints provided by the CROP 04 deep seismic reflection profile (Mazzotti et al., 2007) calibrated with oil-well logs (Patacca, 2007). The box in the map corresponds to the map area of **Fig. 2 A**.

Figure 2. Horizontal (**A**) and vertical (**B**) sections through the P-wave velocity model by De Landro et al. (2022) and earthquake hypocentres (this study) within the Irpinia region. Earthquake hypocentres (shown as white dots) are projected within ±1 km and within ±2 km on either side of the horizontal and vertical sections, respectively. The dimension of hypocentres is related to the local magnitude, as indicated in the legend. The P-wave isovelocity contours are displayed every 0.5 km/s and the thicker ones correspond to the 4.5 km/s, 5 km/s and 5.5 km/s contours. The white line indicates the boundary of resolution of the P-wave velocity model. Locations of the vertical sections in **B** are indicated in the 4 km horizontal section in **A**. Focal mechanisms of event clusters (i.e., composite focal mechanisms; red "beach ball") and single event (dark gray "beach ball"), numbered following the NW-SE direction, are plotted using a lower hemisphere projection in **A** and along vertical planes parallel to the sections in **B**. The dashed red and blue lines are traced approximately through the middle and parallel to the long axis of the wide SW- and NE-dipping hypocentres clusters, respectively.

Figure 3. 5.5 km/s isovelocity surface of the P-wave velocity model by De Landro et al. (2022) within the study area. Note the deepening of low P-wave velocity material from SW to NE, and how this takes place along a curved interface.

Figure 4. 3D block diagram of the central part of the study area built by integrating the new micro-seismicity catalogue of this work, with P-wave velocity (De Landro et al., 2022) and available geological data (Ascione et al., 2013, 2020) data. The diagram comprises two portions displaced for visualization purposes (complete block diagram in the upper left corner). The location of the top vertical section through the middle of the diagram coincides with that of the geological cross-section in **Fig. 1** and with that of section III of **Fig. 2B**, while the bottom section corresponding to the SE side of the block diagram coincides with section IV of **Fig.**

2B. Earthquake hypocentres (shown as white dots) are projected from 2 km on either side of the vertical sections. Focal mechanisms correspond to 4, 6, 7 in **Fig. 2A**, seen in map views.

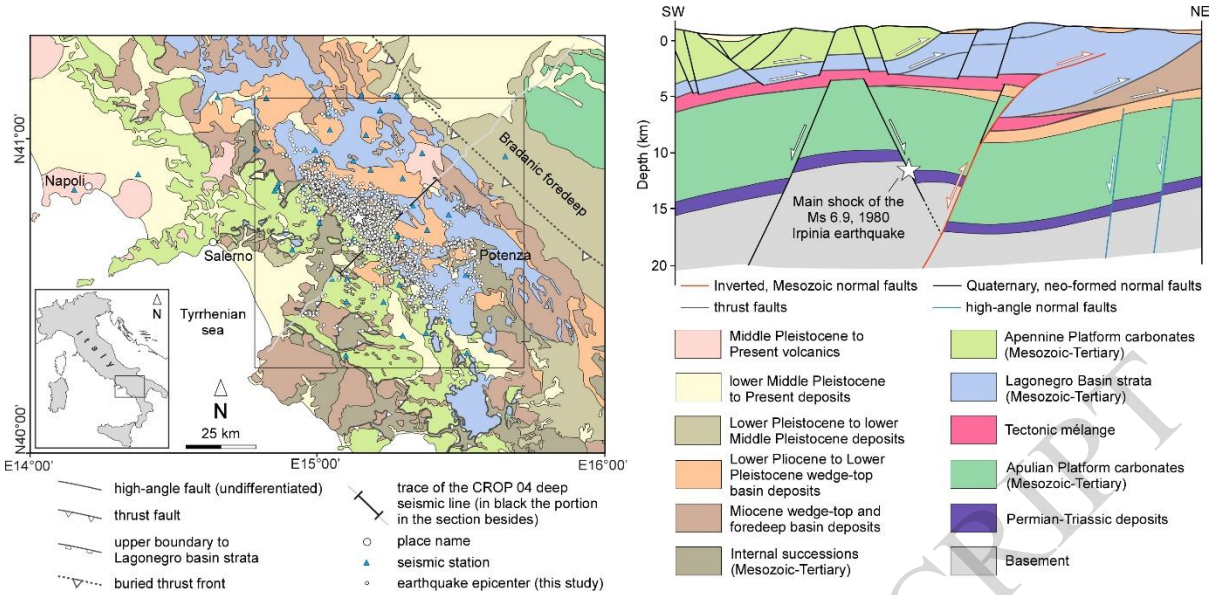

Figure 1

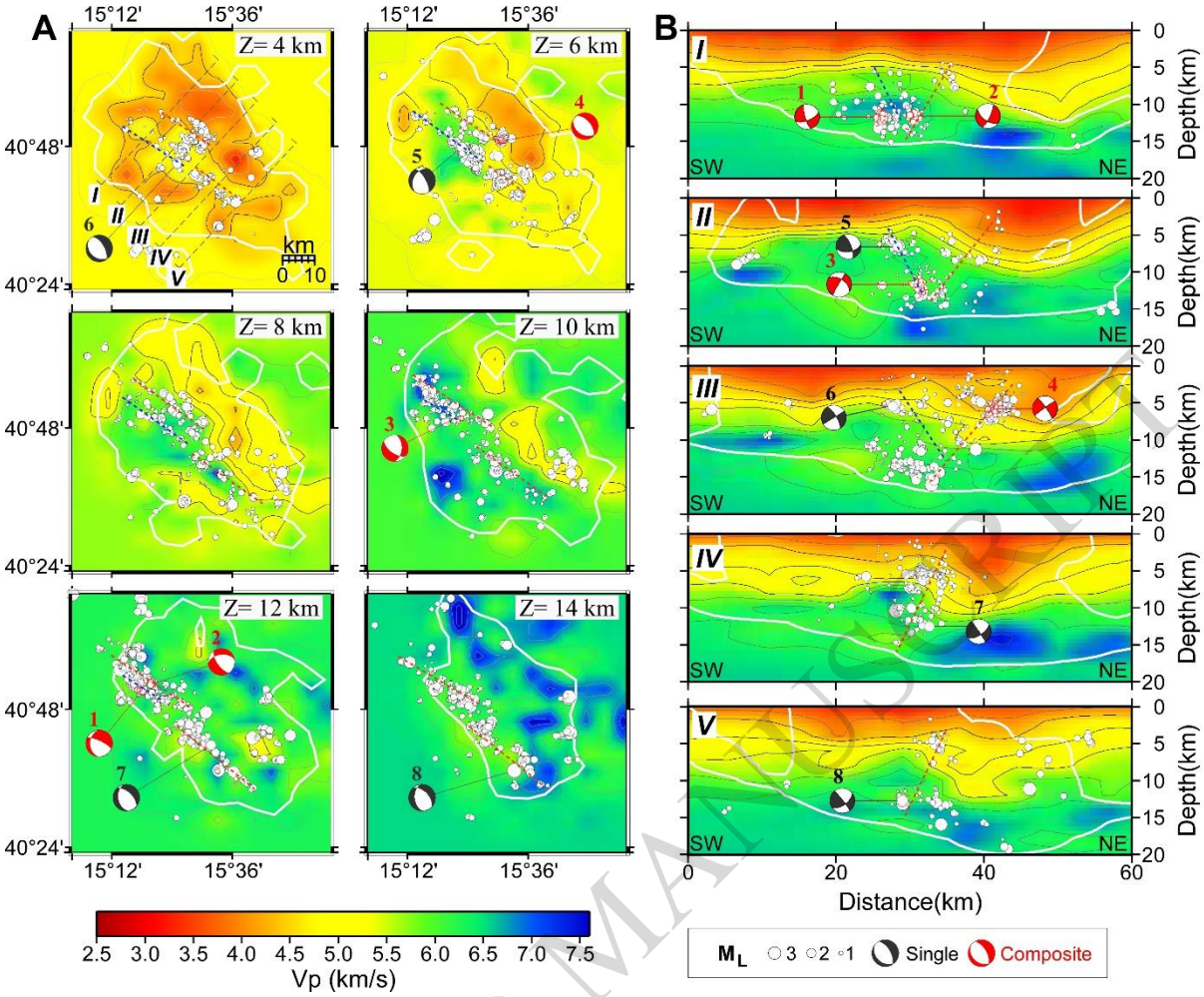

Figure 2

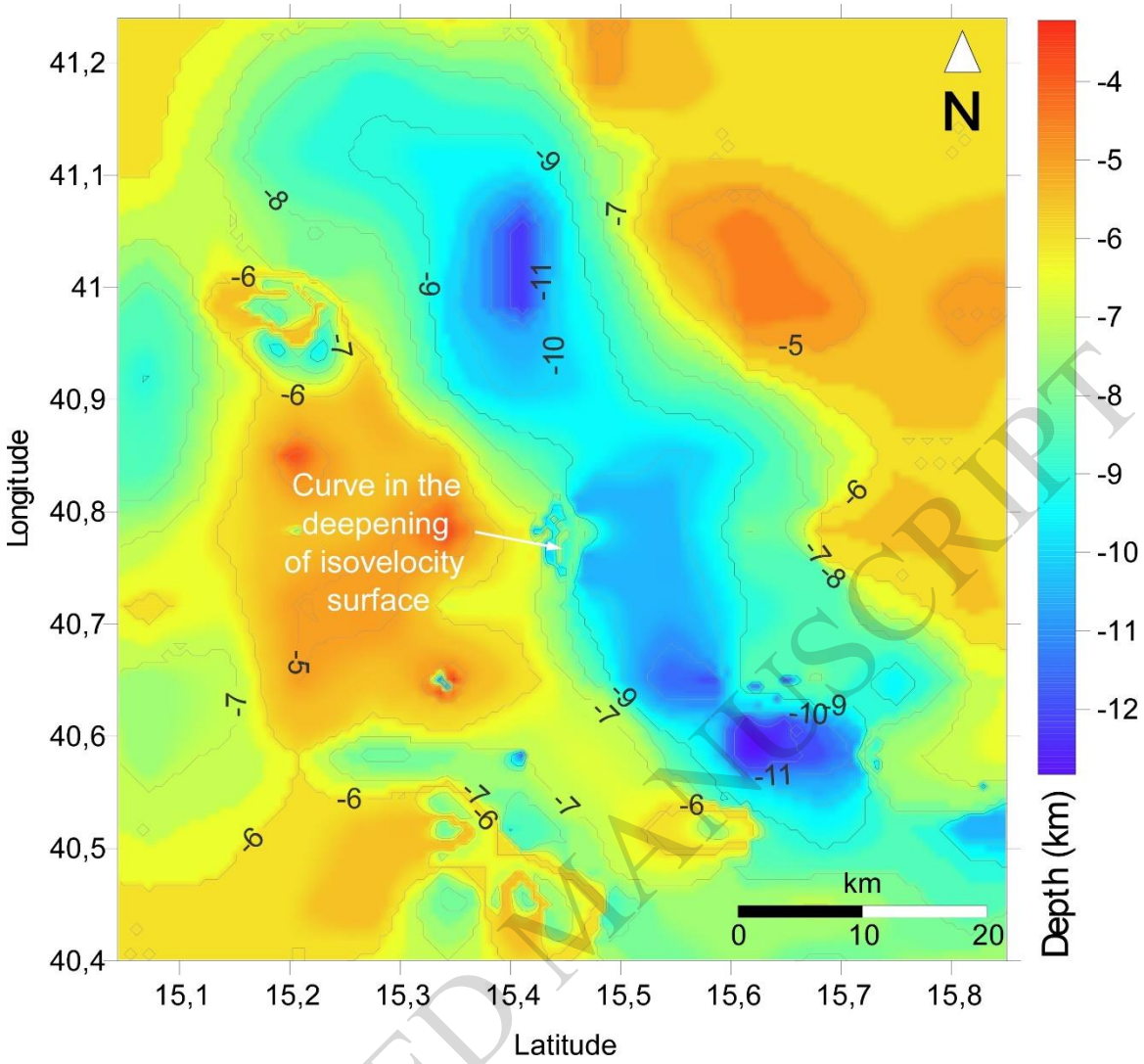

Figure 3

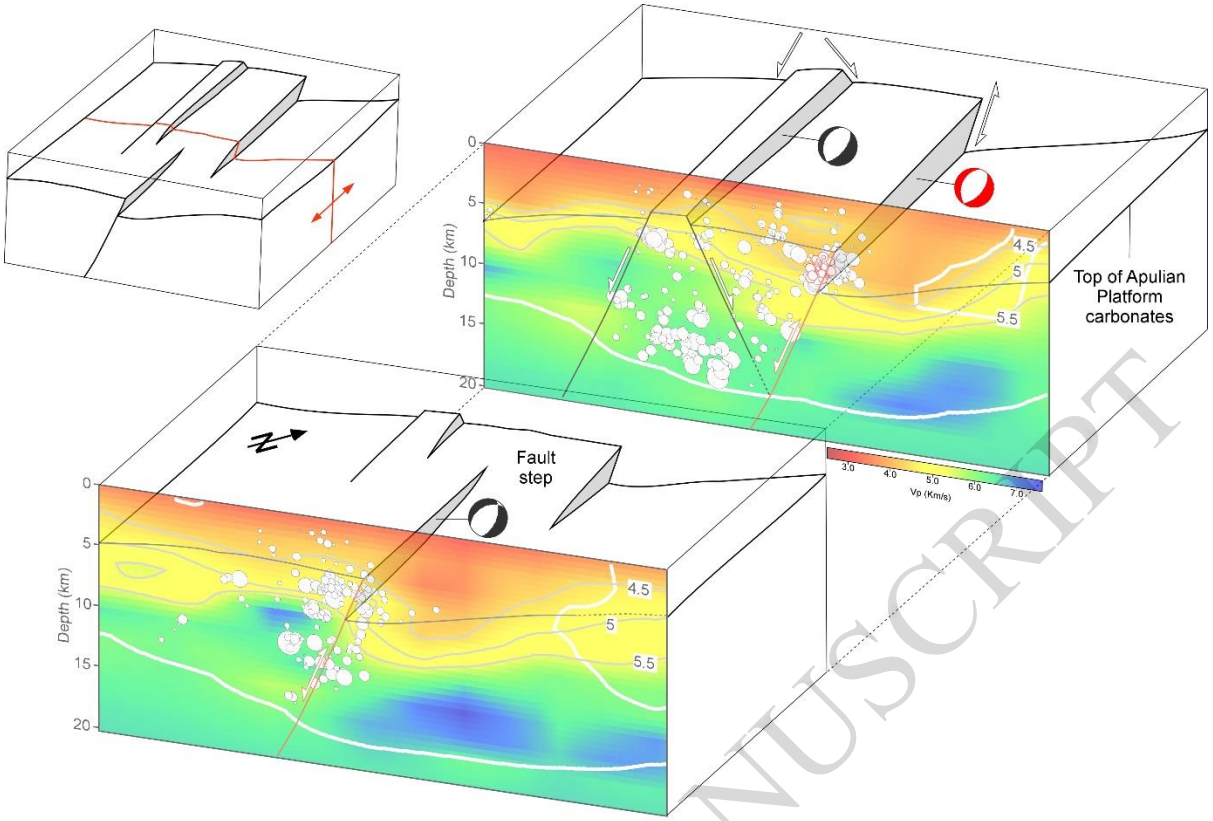

Figure 4